Non-Markovian coherence dynamics of a driven spin-boson model: Damped quantum-beat or large-amplitude coherence oscillation

Xiufeng Cao* and Hang Zheng
Department of Physics, Shanghai Jiao Tong University, Shanghai 200240, People's Republic of China
(Received 11 February 2007; published 29 June 2007)

The dynamics of a driven spin-boson model is studied by means of the perturbation approach based on a unitary transformation. Analytical expressions for the population difference and the coherence of the two state system are obtained. The results show that for weak driving, the population difference displays damping coherent oscillation and/or damping quantum beat, depending on the initial preparation. The coherence exhibits damped oscillation with Rabi frequency. When driving is strong enough, the population difference exhibits undamped large-amplitude coherent oscillation. In addition, our theory leads to correct results in two limiting cases: without dissipation and without driving field.

DOI: 10.1103/PhysRevA.75.062121 PACS number(s): 03.65.Yz, 03.67.Lx, 03.67.Pp

I. INTRODUCTION

Discrete electronic states of qubits can be considered as two state systems (TSS) relating to the potential use of building blocks of prospective quantum logic gates [1,2]. Coupling of solid-state qubits, including superconducting [3–6] and semiconducting [7–10] ones, to environmental degrees of freedom potentially leads to dephasing. The development of techniques to retain coherence in the qubits is a key point for a successful implementation of quantum information processing in these systems.

By means of the development of local spectroscopy techniques, the atomiclike optical properties of semiconductor quantum dots (charge qubit) or a superconducting ring (flux qubit) have been intensively studied. The group of Stievater reported the first observation of Rabi oscillations from excitons confined to a single $GaAs/Al_{0.3}Ga_{0.7}As$ quantum dot (QD) [11]. Besombes *et al.* optically controlled the charge state of a single QD and coherently manipulated the confined wave function to exploit quantum interference and Rabi oscillation phenomena by microspectroscopy in individual InGaAs/GaAs QDs [12]. Using a pulse technique, Pashkin *et al.* coherently mixed quantum states and observed quantum coherent oscillation of coupled qubits in the vicinity of the coresonance [13]. The spectrum of the quantum coherent oscillations reflected interaction between the qubits. Zrenner *et al.* actualized Rabi oscillation by playing an InGaAs quantum dot in a photodiode and demonstrated that coherent optical excitations in the quantum dot can be converted into deterministic photocurrents [14]. While many-body effects of the environment fundamentally change many aspects of Rabi oscillations, the lack of saturation or decoherence is of utmost importance. A good knowledge of the decoherence holds most prominently for many applications such as optoelectronic devices in quantum information processing where the operation completely relies on the presence of coherence [15]. Thereupon, we think over two questions: First, how does the interplay or competition between optical driving and dissipation in the TSS influence the decoherence? Second, can one sustain large-amplitude coherent oscillation in a driven spin-boson model?

The dynamics of a driven spin-boson model [16] has attracted the attention of theoreticians for its widespread applications to various biological, chemical, and physical systems, e.g., ac-driven superconducting quantum interference devices, laser-induced isomerization of bistable molecules, laser-induced localization of electrons in semiconductor double-well quantum structures, or paraelectric resonance. The different communities typically rely on different methods of description. The most direct approach is the portrayal of the time evolution of the reduced density matrix $\rho(t)$ in the generalized master equation (GME) of the TSS. Two popular approaches are based on either the expansion over system-bath coupling by the projecting operator method (commonly known as the Bloch-Redfield formalism) [17], or the expansion over the tunneling Δ by (real-time) path-integral methods such as noninteracting blip approximation (NIBA) [18]. Hartmann *et al.* have illuminated the advantages and disadvantages of these two approaches [19]. A special case where the field frequency is comparable to the TSS tunneling (resonance or near-resonance) is prominently important in experiment, but is more difficult to handle analytically. If the system-bath coupling is weak, the traditional optical Bloch equations will produce a meaningful result [20,21]. However, the constant decoherence rate is too simple to make detailed quantitative predictions [22]. In general, to obtain a solution for time-dependent spin-boson problems even numerically is a nontrivial task [23,24].

In this paper we study the quantum dynamics of a driven spin-boson model, where the frequency of the driven field is resonance to the tunneling in the TSS. Analytical expressions for the population difference $\langle\sigma_z(t)\rangle$ and the coherence $\langle\sigma_x(t)\rangle$ are derived through perturbation treatment based on a unitary transformation. The result shows that with increasing an amplitude of the driving field, the population difference converts damped quantum oscillation (single frequency or double frequency) into large amplitude undamped coherent oscillation. So one can efficiently control quantum coherent dynamic by optical pulse to induce and maintain large-amplitude coherent oscillations. The critical condition from damped to undamped large-amplitude coherent oscillations is

*cxf@sjtu.edu.cn

obtained. We have also investigated the dependence of the population difference $\langle\sigma_z(t)\rangle$ and the coherence $\langle\sigma_x(t)\rangle$ on the initial state.

The paper is organized as follows: In Sec. II we introduce the model Hamiltonian for driven spin-boson coupling and solve it in terms of a perturbation treatment based on unitary transformation. The dependence of the population difference and the coherence on the initial conditions and the strength of the driving field are discussed in Sec. III. Finally, the conclusion is given in Sec. IV.

II. MODEL AND THEORY

We study the dynamics of a driven spin-boson, where the two state system is linearly coupled to a heat bath and is driven by a classical microwave field. The system can be modeled by the Hamiltonian [18,21] as follows:

$$H(t) = H_s + H_d(t) + H_b + H_i, \tag{1}$$

with

$$H_s = -\Delta\sigma_x/2, \tag{2}$$

$$H_d(t) = \varepsilon(t)\sigma_z, \tag{3}$$

$$H_b = \sum_k \omega_k b_k^\dagger b_k, \tag{4}$$

$$H_i = \frac{1}{2}\sum_k g_k(b_k^\dagger + b_k)\sigma_z, \tag{5}$$

where H_s is the Hamiltonian of the TSS, $H_d(t)$ is the external driven field, H_b is the bath, and H_i is the bath system interaction responding for decoherence. Throughout this paper we set $\hbar=1$. Here σ_i $(i=x,y,z)$ are Pauli spin matrices, Δ describes the tunneling coupling between the two states, and $\varepsilon(t)$ is the external time-dependent modulating field. $b_k^\dagger$ (b_k) and ω_k are the creation (annihilation) operator and energy of the phonons with the wave vector k. g_k is the electron-phonon coupling strength. In this work we consider the zero bias and zero temperature case. The bath is completely defined by the spectral density as follows:

$$J(\omega) = \sum_k g_k^2\delta(\omega-\omega_k). \tag{6}$$

We consider the Ohmic bath $J(\omega)=2\alpha\omega\theta(\omega_c-\omega)$ in this work, where α is the dimensionless coupling constant and $\theta(x)$ is the usual step function.

First, we diagonalize the time-independent part of the Hamiltonian $H_s+H_b+H_i$. Apply a canonical transformation $H'=\exp(s)H\exp(-s)$ with the generator [25] as follows:

$$S = \sum_k \frac{g_k}{2\omega_k}\xi_k(b_k^\dagger - b_k)\sigma_z. \tag{7}$$

Then decompose the transformed Hamiltonian H' into three parts as follows:

$$H' = H_0' + H_1' + H_2', \tag{8}$$

where

$$H_0' = -\frac{1}{2}\eta\Delta\sigma_x + \sum_k \omega_k b_k^\dagger b_k - \sum_k \frac{g_k^2}{4\omega_k}\xi_k(2-\xi_k), \tag{9}$$

$$H_1' = -\frac{1}{2}\sum_k g_k(1-\xi_k)(b_k^\dagger + b_k)\sigma_x - i\frac{\eta\Delta}{2}\sigma_y\sum_k \frac{g_k}{\omega_k}\xi_k(b_k^\dagger - b_k), \tag{10}$$

$$H_2' = -\frac{1}{2}\Delta\sigma_x\left[\cosh\left(\sum_k \frac{g_k}{\omega_k}\xi_k(b_k^\dagger - b_k)\right) - \eta\right] - i\frac{\Delta}{2}\sigma_y\left[\sinh\left(\sum_k \frac{g_k}{\omega_k}\xi_k(b_k^\dagger - b_k)\right) - \eta\sum_k \frac{g_k}{\omega_k}\xi_k(b_k^\dagger - b_k)\right], \tag{11}$$

with

$$\eta = \exp\left(-\sum_k \frac{g_k^2}{2\omega_k^2}\xi_k^2\right), \tag{12}$$

$$\xi_k = \frac{\omega_k}{\omega_k + \eta\Delta}. \tag{13}$$

Obviously, H_0' can be solved exactly. We denote the ground state of H_0' as $|g\rangle=|s_1\rangle|\{0_k\}\rangle$, and the lowest excited states as $|s_2\rangle|\{0_k\}\rangle$, $|s_1\rangle|\{1_k\}\rangle$, where $|s_1\rangle$ and $|s_2\rangle$ are eigenstates of σ_x ($\sigma_x|s_1\rangle=|s_1\rangle$, $\sigma_x|s_2\rangle=-|s_2\rangle$), while $|\{n_k\}\rangle$ means that there are n_k phonons for mode k. The last term of H_0' is a constant and has no effect on the dynamics behavior. It is easy to check that $\langle g|H_2'|g\rangle=0$ (because of the form of η), $\langle\{0_k\}|\langle s_2|H_2'|g\rangle=0$, $\langle\{1_k\}|\langle s_1|H_2'|g\rangle=0$, and $\langle\{0_k\}|\langle s_2|H_2'|s_1\rangle|\{1_k\}\rangle=0$. Moreover, $\langle\{0_k\}|\langle s_2|H_1'|g\rangle=0$ and $\langle\{1_k\}|\langle s_1|H_1'|g\rangle=0$. Thus, we can diagonalize the lowest excited states of H' as

$$H' = -\frac{1}{2}\eta\Delta|g\rangle\langle g| + \sum_E E|E\rangle\langle E|. \tag{14}$$

The diagonalization is through the following transformations [25]:

$$|s_2\rangle|\{0_k\}\rangle = \sum_E x(E)|E\rangle, \tag{15}$$

$$|s_1\rangle|\{1_k\}\rangle = \sum_E y_k(E)|E\rangle, \tag{16}$$

$$|E\rangle = x(E)|s_2\rangle|\{0_k\}\rangle + \sum_k y_k(E)|s_1\rangle|\{1_k\}\rangle, \tag{17}$$

where

$$x(E) = \left[1 + \sum_k \frac{V_k^2}{\left(E + \frac{1}{2}\eta\Delta - \omega_k\right)^2}\right]^{-1/2}, \tag{18}$$

and

$$y_k(E) = \frac{V_k}{E + \frac{1}{2}\eta\Delta - \omega_k} x(E), \tag{19}$$

with $V_k = \eta\Delta g_k \xi_k / \omega_k$. E's are the diagonalized excitation energy satisfying the following eigenvalue equation:

$$E - \frac{1}{2}\eta\Delta - \sum_k \frac{V_k^2}{E + \frac{1}{2}\eta\Delta - \omega_k} = 0. \tag{20}$$

A series of experiments has successfully realized coherent control of the qubit by applying resonant microwave excitations [3]. Among them, qubit is driven by a time-dependent term $\varepsilon_{mw}\cos(2\pi Ft)\sigma_z$, where F is the microwave frequency and ε_{mw} is the microwave amplitude. In view of the experiments, we focus our attention on a monochromatic field of the form $\varepsilon(t) = \varepsilon\cos(\Omega t)$ and choose the control field excitation to be resonant with the tunneling of TSS. Since σ_z is commutative with S, the total transformed Hamiltonian approximately reads

$$H' = -\frac{1}{2}\eta\Delta|g\rangle\langle g| + \sum_E E|E\rangle\langle E| - \varepsilon\cos(\Omega t)\sigma_z. \tag{21}$$

After expanding in the eigenstates $|g\rangle$ and $|E\rangle$,

$$H' = -\frac{1}{2}\eta\Delta|g\rangle\langle g| + \sum_E E|E\rangle\langle E| - \frac{\varepsilon}{2}\sum_E [x^*(E)|g\rangle\langle E|\exp(i\Omega t) + x(E)|E\rangle\langle g|\exp(-i\Omega t)]. \tag{22}$$

In deriving Eq. (22), we have ignored the counterrotating terms [26]. This is generally a very good approximation, especially in the special case when the two states are at resonance or near resonance with the incident field $\Delta \approx \Omega$. In the interaction picture,

$$H_0' = -\frac{1}{2}\eta\Delta|g\rangle\langle g| + \sum_E E|E\rangle\langle E|, \tag{23}$$

$$V_I(t) = -\frac{\varepsilon}{2}\sum_E \left\{ x^*(E)|g\rangle\langle E|\exp\left[i\left(-\frac{1}{2}\eta\Delta - E + \Omega\right)t\right] + x(E)|E\rangle\langle g|\exp\left[-i\left(-\frac{1}{2}\eta\Delta - E + \Omega\right)t\right]\right\}. \tag{24}$$

The wave function in an interaction picture can be written as $|\Psi(t)\rangle = C_1(t)|g\rangle + \Sigma_E C_E(t)|E\rangle$, where $|C_1(t)|^2$ and $|C_E(t)|^2$ are the probability of finding the particle in states $|g\rangle$ and $|E\rangle$ at time t, respectively. The equation of motion in the interaction picture is

$$\frac{d}{dt}|\Psi(t)\rangle = -iV_I(t)|\Psi(t)\rangle. \tag{25}$$

Suppose the initial state is $\exp(S)|\Psi(0)\rangle = C_1(0)|s_1\rangle|\{0_k\}\rangle + C_2(0)|s_2\rangle|\{0_k\}\rangle = C_1(0)|g\rangle + C_2(0)\Sigma_E x(E)|E\rangle$. After Laplace transformation, the solution of Eq. (25) is

$$C_1(P) = \frac{C_1(0) + \frac{\varepsilon}{2}C_2(0)\sum_E \frac{|x(E)|^2}{E - iP}}{P + i\left(-\frac{1}{2}\eta\Delta + \Omega\right) - i\frac{\varepsilon^2}{4}\sum_E \frac{|x(E)|^2}{E - iP}}, \tag{26}$$

and

$$\sum_E x^*(E)C_E(P) = \frac{-i\sum_E \frac{|x(E)|^2}{E - iP}\left\{C_2(0)\left[P + i\left(-\frac{1}{2}\eta\Delta + \Omega\right)\right] + i\frac{\varepsilon}{2}C_1(0)\right\}}{P + i\left(-\frac{1}{2}\eta\Delta + \Omega\right) - i\frac{\varepsilon^2}{4}\sum_E \frac{|x(E)|^2}{E - iP}}. \tag{27}$$

By contour integration in the complex function theory, the summation over E's can be simplified (see the Appendix) as follows:

$$\sum_E \frac{|x(E)|^2}{E - iP} = -\frac{1}{iP - \frac{1}{2}\eta\Delta - \sum_k \frac{V_k^2}{iP + \frac{1}{2}\eta\Delta - \omega_k}}. \tag{28}$$

Substituting it into Eqs. (26) and (27),

$$C_1(P)=\frac{C_1(0)\left(iP-\frac{1}{2}\eta\Delta-\sum_k\frac{V_k^2}{iP+\frac{1}{2}\eta\Delta-\omega_k}\right)+\frac{\varepsilon}{2}C_2(0)}{\left[P+i\left(-\frac{1}{2}\eta\Delta+\Omega\right)\right]\left(iP-\frac{1}{2}\eta\Delta-\sum_k\frac{V_k^2}{iP+\frac{1}{2}\eta\Delta-\omega_k}\right)+i\frac{\varepsilon^2}{4}}, \tag{29}$$

$$\sum_E x^*(E)C_E(P)=\frac{C_2(0)\left(iP+\frac{1}{2}\eta\Delta-\Omega\right)-\frac{\varepsilon}{2}C_1(0)}{\left[P+i\left(-\frac{1}{2}\eta\Delta+\Omega\right)\right]\left(iP-\frac{1}{2}\eta\Delta-\sum_k\frac{V_k^2}{iP+\frac{1}{2}\eta\Delta-\omega_k}\right)+i\frac{\varepsilon^2}{4}}. \tag{30}$$

Then, changing $iP+\frac{1}{2}\eta\Delta$ to $\omega+i0^+$ [27], $C_1(P)$ and $\Sigma_E x^*(E)C_E(P)$ can be rewritten as

$$C_1(\omega)=\frac{iC_1(0)[\omega-\eta\Delta-R(\omega)+i\gamma(\omega)]-i\frac{\varepsilon}{2}C_2(0)}{(\omega-\Omega)[\omega-\eta\Delta-R(\omega)+i\gamma(\omega)]-\frac{\varepsilon^2}{4}}, \tag{31}$$

and

$$\sum_E x^*(E)C_E(\omega)=\frac{iC_2(0)(\omega-\Omega)-i\frac{\varepsilon}{2}C_1(0)}{(\omega-\Omega)[\omega-\eta\Delta-R(\omega)+i\gamma(\omega)]-\frac{\varepsilon^2}{4}}, \tag{32}$$

where $R(\omega)$ and $\gamma(\omega)$ denote the real and imaginary parts of $\Sigma_k V_k^2/(\omega-\omega_k)$,

$$\begin{aligned}R(\omega)&=\sum_k \wp\frac{V_k^2}{\omega-\omega_k}=(\eta\Delta)^2\wp\int_0^\infty d\omega'\frac{J(\omega')}{(\omega-\omega')(\omega'+\eta\Delta)^2}\\&=-2\alpha\frac{(\eta\Delta)^2}{\omega+\eta\Delta}\left\{\frac{\omega_c}{\omega_c+\eta\Delta}-\frac{\omega}{\omega+\eta\Delta}\ln\left[\frac{|\omega|(\omega_c+\eta\Delta)}{\eta\Delta(\omega_c-\omega)}\right]\right\},\end{aligned} \tag{33}$$

and

$$\begin{aligned}\gamma(\omega)&=\pi\sum_k V_k^2\delta(\omega-\omega_k)=\pi(\eta\Delta)^2\frac{J(\omega)}{(\omega+\eta\Delta)^2}\\&=2\alpha\pi\omega\frac{(\eta\Delta)^2}{(\omega+\eta\Delta)^2},\quad 0\le\omega\le\omega_c,\end{aligned} \tag{34}$$

where $\wp$ stands for the Cauchy principal value. Compared with Bloch equation and Markovian approximation, decoherence rates $\gamma(\omega)$ in our results are frequency dependent. That is more general and physical.

We inverse the Laplace transformation,

$$C_1(t)=\frac{\exp(i\eta\Delta t/2)}{2\pi}\int_{-\infty}^{+\infty}C_1(\omega)\exp(-i\omega t+0^+)d\omega, \tag{35}$$

$$\sum_E x^*(\omega)C_E(t)=\frac{\exp(i\eta\Delta t/2)}{2\pi}\int_{-\infty}^{+\infty}\sum_E x^*(\omega)C_E(\omega)\times\exp(-i\omega t+0^+)d\omega. \tag{36}$$

The expectation value of σ_i $(i=x,z)$ can be expressed as

$$\langle\sigma_i(t)\rangle=\langle\Psi(t)|\sigma_i(t)|\Psi(t)\rangle=\langle\Psi(0)|\exp(-S)\exp(-iH't)\sigma_i\exp(iH't)\exp(S)|\Psi(0)\rangle. \tag{37}$$

After straightforward calculation, the analytical expression for the population difference $\langle\sigma_z(t)\rangle$ and the coherence $\langle\sigma_x(t)\rangle$ are

$$\langle\sigma_z(t)\rangle=2\,\mathrm{Re}\left(C_1^*(t)\sum_E x^*(\omega)C_E(t)\exp(-i\Omega t)\right) \tag{38}$$

and

$$\langle\sigma_x(t)\rangle=\eta^*\left(1-2\sum_E x^*(\omega)C_E(t)\sum_{E'}x^*(\omega)C_{E'}(t)\right). \tag{39}$$

III. RESULTS AND DISCUSSION

Here, we are going to discuss the two limiting cases of considered Hamiltonian: without dissipation and without driving field. First, without the coupling to bath, our Hamiltonian Eq. (1) is the same as that of the driving two-level model in quantum optics [26], if we substitute σ_x in Eq. (1) by σ_z and σ_z by σ_x. As is well known, the model dynamics in quantum optics depends on the initial condition. In the notation of Eq. (1) the dynamics without the coupling to bath can be described as follows: If the initial preparation is $\langle\sigma_x(t$

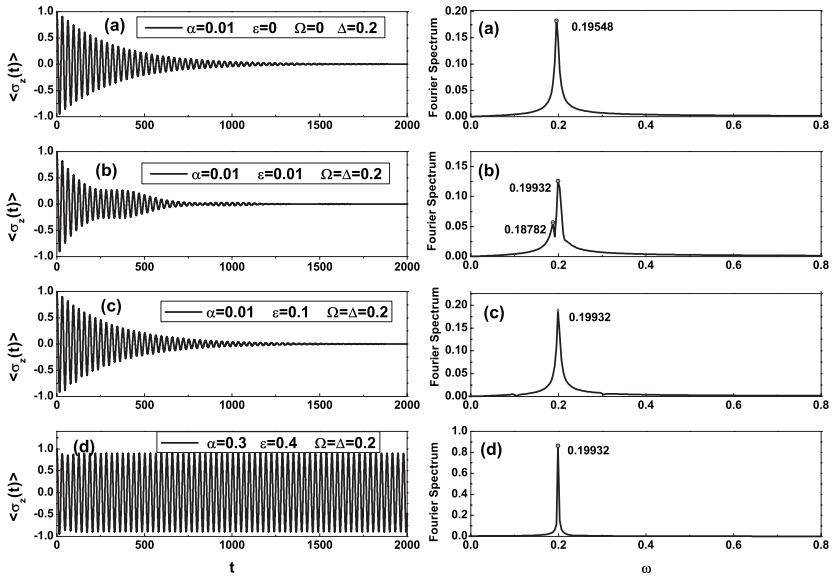

FIG. 1. The population difference $\langle\sigma_z(t)\rangle$ as a function of t for the initial condition $\langle\sigma_z(t=0)\rangle=1$ with various values of the driving field amplitude (left panels), $\varepsilon=0$ (a), 0.01 (b), 0.1 (c), and 0.4 (d). Also shown in the right panels are the corresponding frequency spectra with the same parameters as in left ones. The coupling is $\alpha=0.01$ except (d) $\alpha=0.3$. The driving field frequency is in resonance with TSS $\Omega=\Delta$. Here and in the following figures ε, Δ, and frequency Ω are expressed in units of ω_c and time in units of ω_c^{-1}.

$=0)\rangle=1$ and the driven field is turned on, the population difference $\langle\sigma_z(t)\rangle$ displays quantum beat that results from the interference of fast oscillation with field frequency Ω and slow oscillations with Rabi frequency ε. The coherence $\langle\sigma_x(t)\rangle$ oscillates with the Rabi frequency. But if the system is initially in the state $\langle\sigma_z(t=0)\rangle=1$, without the bath $\langle\sigma_z(t)\rangle$ oscillates as $\cos\Omega t$ but $\langle\sigma_x(t)\rangle=0$. Second, it is also known that $\langle\sigma_z(t)\rangle$ damply oscillates if the coupling system Eq. (1) lacks the driven field [25]. Our purpose in this paper is to study how the dissipative environment and driven field determine collectively the quantum dynamics of TSS.

We discuss mainly the resonant case $\Omega=\Delta$. ω_c is taken as the energy unit and time is in units of ω_c^{-1}. The coupling to the bath is taken as $\alpha=0.01$ in all calculations except Fig. 1(d), $\alpha=0.3$. In Fig. 1, we plot the population difference $\langle\sigma_z(t)\rangle$. The initial state is $\langle\sigma_z(t=0)\rangle=1$ with bath in thermal equilibrium. The curves shown in panels (a), (b), and (c) correspond to three different amplitudes of external field $\varepsilon=0$, 0.01, 0.1. Figure 1(d) presents the population difference $\langle\sigma_z(t)\rangle$ with $\varepsilon=0.4$ and $\alpha=0.3$. The Fourier spectrums of $\langle\sigma_z(t)\rangle$ are presented in the right four panels, respectively. As seen from Fig. 1(a), without driving, the population difference exhibits damped oscillation. The oscillation frequency ω_0 and the damping rate γ well agree with previous results [25]. Figure 1(b) shows the case of weak driving where $\langle\sigma_z(t)\rangle$ decays with beat pattern of two frequencies at about $\Omega-\varepsilon$ and Ω. Further increasing driving strength, $\langle\sigma_z(t)\rangle$ damply oscillates with a master frequency Ω in Fig. 1(c). These three cases show that in the weak driving case, the system always damply oscillates and this genuine quantum coherence oscillation is weakened by friction from the dissipative bath. In Fig. 1(d), for sufficiently strong amplitude $\varepsilon\geq 2\Omega$, population difference damply oscillates with a short time at the beginning, then displays undamped large-amplitude coherent oscillation with the frequency of the driving field Ω. In order to see the process clearly, we choose strong coupling $\alpha=0.3$. In this case, the driving field overcomes dissipation and dominates the dynamics of the system. Comparing Figs. 1(a)–1(d), we can see that the population difference $\langle\sigma_z(t)\rangle$ displays a quantum beat only for the weak

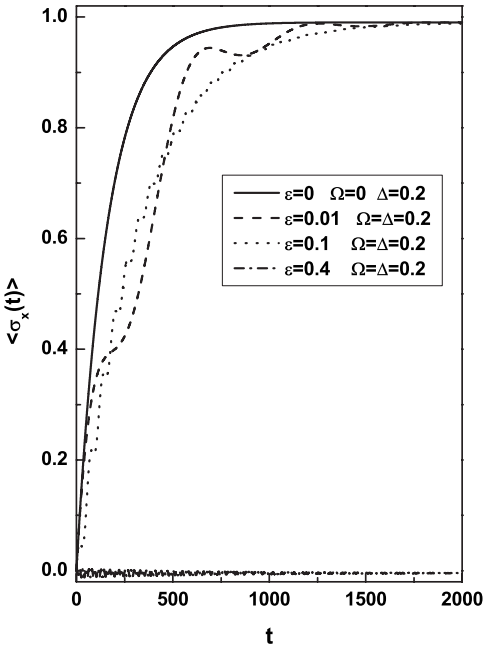

FIG. 2. The coherence $\langle\sigma_x(t)\rangle$ as a function of t for the initial condition $\langle\sigma_z(t=0)\rangle=1$ with various values of the driving field amplitude, $\varepsilon=0$ (solid line), 0.01 (dashed line), 0.1 (dotted line), and 0.4 (dot-dashed line). The coupling is $\alpha=0.01$ and the other parameters are the same as in Fig. 1.

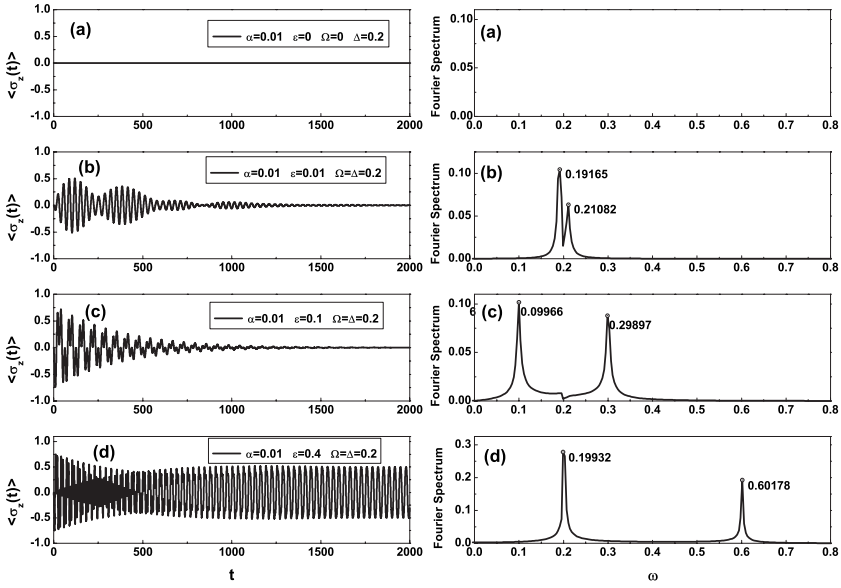

FIG. 3. The population difference $\langle\sigma_z(t)\rangle$ as a function of t for the initial condition $\langle\sigma_x(t=0)\rangle=1$ with various values of the driving field amplitude (left panels), $\varepsilon=0$(a), 0.01(b), 0.1(c), and 0.4(d). Also shown in the right panels are the corresponding frequency spectra with the same parameters as in the left ones. The coupling is $\alpha=0.01$. The driving field frequency is in resonance with TSS $\Omega=\Delta$.

driving case: $\Omega-\gamma\leq|\Omega\pm\varepsilon|\leq\Omega+\gamma$, as where γ is the damping rate.

In Fig. 2, the coherence $\langle\sigma_x(t)\rangle$ is plotted with $\alpha=0.01$ and the other parameters are the same as in Fig. 1. Without driving, the coherence $\langle\sigma_x(t)\rangle$ asymptotically goes to 1, implying that the system decays to the ground state for a long time [28]. For weak driving amplitude $\varepsilon=0.01$ and 0.1, it is visible that $\langle\sigma_x(t)\rangle$ tends to 1 with the oscillation of Rabi frequency ε. While for large driven field strength $\varepsilon=0.4$, the coherence $\langle\sigma_x(t)\rangle$ oscillates around zero with a small amplitude. The driving makes the occupation probability on the two states equal, that is to say, the electron tunnels frequently between the two states and the strong driving field suppresses the effect of the dissipative environment.

Any superposition $|\Psi\rangle=\alpha|s_1\rangle+\beta|s_2\rangle$ can be prepared in experiment, through manipulation of the quantum state by applying microwave pulses $\mu(t)$ to the gate [29]. Figure 3 shows the population difference $\langle\sigma_z(t)\rangle$ for the same parameters as in Fig. 2, but with different initial condition $\langle\sigma_x(t=0)\rangle=1$. Without driving, $\langle\sigma_z(t)\rangle=0$ in Fig. 3(a). For weak driving, despite the dissipation, Rabi oscillations can be induced by applying microwave field in resonance with the TSS. The oscillation decays nonexponentially and displays a clear beating. From the frequency spectrum (right panels), one can see the two peaks at around $\Omega-\varepsilon$ and $\Omega+\varepsilon$, that is to say, $\langle\sigma_z(t)\rangle$ can be fitted by $\sin\varepsilon t*\sin\Omega t$. It is the well-known quantum beat in quantum optics, but here the beat is dissipative. In Fig. 3(d), well-behaved coherent oscillation can be observed when the driving field strength is adequately strong $\varepsilon=0.4$. The frequency of the oscillation is $\Omega+\varepsilon$ and Ω.

With the same parameters and the initial condition as in Fig. 3, the coherence $\langle\sigma_x(t)\rangle$ is plotted in Fig. 4. The coherence $\langle\sigma_x(t)\rangle$ displays damped oscillation with Rabi frequency and finally stabilizes in the ground state in Figs. 4(a) and 4(b). The damping can be treated as a leakage of energy [30] and the leakage may be suppressed by enhancement of the driving field. For strong driving, the long time limit shifts to a different value because of the external field.

It has been observed in experiment that the population difference $\langle\sigma_z(t)\rangle$ may display a damping quantum beat in

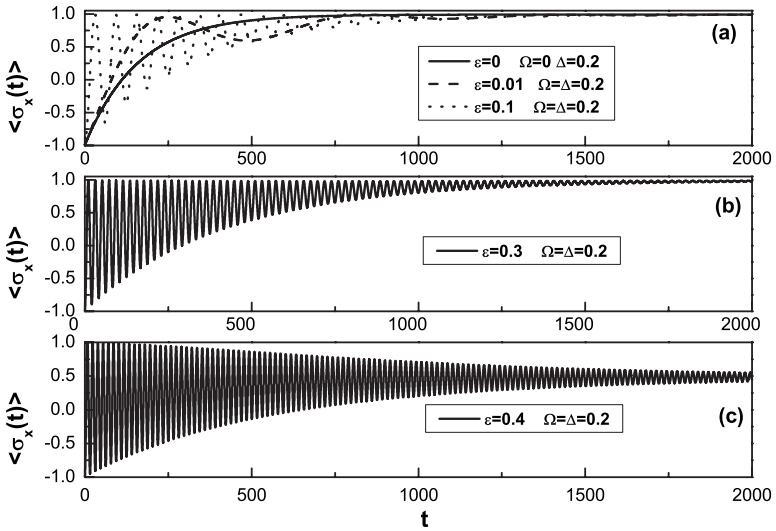

FIG. 4. The coherence $\langle\sigma_x(t)\rangle$ as a function of t for the initial condition $\langle\sigma_x(t=0)\rangle=1$ with various values of the driving field amplitude. (a) $\varepsilon=0$ (solid line), 0.01 (dashed line), and 0.1 (dotted line), (b) 0.3, (c) 0.4. The other parameters are the same as in Fig. 3.

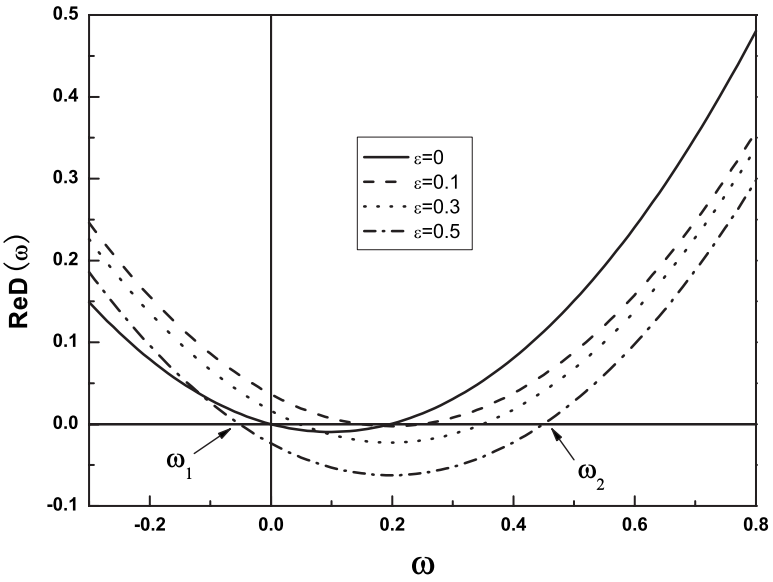

FIG. 5. Re $D(\omega)$ vs ω for the different driving field amplitude $\varepsilon=0$ (solid line), 0.1 (dashed line), 0.3 (dotted line), and 0.5 (dot-dashed line).

the superconducting qubit [3]. Comparing two cases of quantum beat in Figs. 1 and 3, our calculations show that the initial condition of TSS determines the features of the quantum beat. First, the condition for the beat to appear in the initial preparation of Fig. 1 is more rigorous than in that of Fig. 3. In the initial condition of Fig. 1 the quantum beat only emerges in the weak driving case and the driving frequency must be in the range of $\Omega-\gamma\leq|\Omega\pm\varepsilon|\leq\Omega+\gamma$, where γ is the damping rate. While in the initial condition of Fig. 3, the quantum beat can always exist, even the driving amplitude is strong enough leading to the undamped oscillation. Next, the frequencies of the beat pattern are Ω and $\Omega-\varepsilon$ (and/or $\Omega+\varepsilon$) in Fig. 1, while in Fig. 3 they are $\Omega-\varepsilon$ and $\Omega+\varepsilon$. The difference of the beating frequencies can be understood as follows. In the initial condition $\langle\sigma_z(t=0)\rangle=1$, $H_d(t)=\varepsilon(t)\sigma_z$ is the maximum and the driven dominates the oscillation of TSS at the beginning, then the environment and driven field interplay. It is natural that the frequency of driving, Ω, is of priority and the quantum beat (double frequencies) can emerge only in the weak driving case. But in the initial condition $\langle\sigma_x(t=0)\rangle=1$, $H_d(t)$ is zero at first and the effects of driving and the environment are equivalent, so the frequencies of the oscillation are $\Omega-\varepsilon$ and $\Omega+\varepsilon$.

In what follows, we discuss the possibility and the critical condition to induce and maintain the long time coherent oscillation by applying a resonant control field. From Eqs. (35), (36), and the theory of complex function, it is known that the behavior of the population difference $\langle\sigma_z(t)\rangle$ and the coherence $\langle\sigma_x(t)\rangle$ can be learned from a study of the poles of $C_1(\omega)$ and $\Sigma_E x^*(\omega)C_E(\omega)$ [Eqs. (31) and (32)]. $C_1(\omega)$ and $\Sigma_E x^*(\omega)C_E(\omega)$ have the same poles, denoted as $D(\omega)=(\omega-\Omega)[\omega-\eta\Delta-R(\omega)+i\gamma(\omega)]-\varepsilon^2/4$, since they have the same denominator. Figure 5 shows the real part of the denominator, $\mathrm{Re}\,D(\omega)=(\omega-\Omega)[\omega-\eta\Delta-R(\omega)]-\varepsilon^2/4$, which is an even function of the driving field ε. When $\varepsilon=0$, the roots of $\mathrm{Re}\,D(\omega)=0$ are at $\omega_1=0$ and $\omega_2=\omega_0$, where ω_0 is the root of equation $\omega-\eta\Delta-R(\omega)=0$ [25] and $\Delta-\omega_0$ is the Lamb shift due to the coupling to bath. Applying driving field to TSS, the two roots of $\mathrm{Re}\,D(\omega)=0$ are shifted. With increasing ε, ω_1 increases first and then goes down, and becomes negative $\omega_1<0$ for larger $\varepsilon\geq2\Omega$. ω_2 increases with increasing ε. Besides, the imaginary part of the denominator, $\mathrm{Im}\,D(\omega)=\gamma(\omega)(\omega-\Omega)$, depends on the frequency ω and plays the role of damping rate. We note that $\gamma(\omega)>0$ for $0\leq\omega\leq\omega_c$ and $\gamma(\omega)=0$ otherwise. Thus, there are two different cases according to whether ω_1 and ω_2 are within the range $0\leq\omega_1$, $\omega_2\leq\omega_c$ or not.

(1) If they are in the range of $0\leq\omega_1$, $\omega_2\leq\omega_c$, then $\gamma(\omega_1)>0$ and $\gamma(\omega_2)>0$ and the poles of $C_1(\omega)$ and $\Sigma_E x^*(\omega)C_E(\omega)$ are on the complex plane away from the real axis. In this case, the dissipation dominates the long time behavior of the system and, after adequate time, the coherent oscillation is damped out.

(2) If ω_1 or ω_2 is outside of the $0\leq\omega_1$, $\omega_2\leq\omega_c$, i.e., ω_1 is negative or $\omega_2>\omega_c$, then the corresponding damping rate vanishes. $\langle\sigma_z(t)\rangle$ cannot decay to zero and may display large-amplitude coherent oscillation. Approximately, we estimate that when $\varepsilon\geq2\Omega$, $\langle\sigma_z(t)\rangle$ can maintain undamped coherence oscillation.

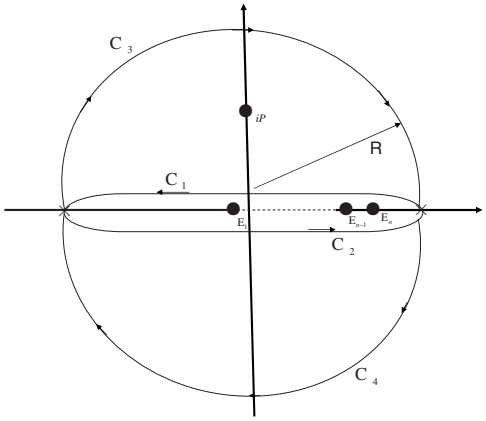

FIG. 6. The contour and the poles in the complex plane.

IV. CONCLUSION

In this paper, we have investigated the quantum driving dynamics of a spin-boson model by a perturbation treatment based on a unitary transformation. The population difference and the coherence are obtained explicitly and analytically. Our approach is not restricted to a special form of spectral density and can be used to study the quantum dynamics of general initial preparation. Additionally, a simple expression for the poles, $(\omega-\Omega)[\omega-\eta\Delta-R(\omega)+i\gamma(\omega)]-\varepsilon^2/4$, allows us to analyze the critical condition from a damped quantum oscillation to an undamped one. We find that, for weak driving, the population difference $\langle\sigma_z(t)\rangle$ displays damping quantum beat, while for strong field $\varepsilon \geq 2\Omega$, $\langle\sigma_z(t)\rangle$ can preserve large-amplitude coherent oscillation. We believe these results may be helpful for quantum information processing and quantum computation where a sufficiently long coherent time is necessary for both the storage and manipulation of the quantum states that are unavoidably exposed to their surrounding environment.

ACKNOWLEDGMENT

This work was supported by the China National Natural Science Foundation (Grants No. 10474062 and No. 90503007).

APPENDIX

In this Appendix, we show details of how to sum over a series of diagonalized excitation energy $E_1, E_2, \ldots, E_{n-1}, E_n,$. First, we construct a contour integral in the complex plane [27] as follows:

$$\sum_E \frac{|x(E)|^2}{E-iP} = \frac{1}{2\pi i}\oint_{C_1+C_2} \frac{dE}{\left(E-\frac{1}{2}\eta\Delta-\sum_k \frac{V_k^2}{E+\frac{1}{2}\eta\Delta-\omega_k}\right)(E-iP)}. \tag{A1}$$

The contour C_1+C_2 is shown in Fig. 6. The denominator $\left(E-\frac{1}{2}\eta\Delta-\Sigma_k\frac{V_k^2}{E+\frac{1}{2}\eta\Delta-\omega_k}\right)(E-iP)$ has real poles $E_1, E_2, \ldots, E_{n-1}, E_n$, on real axis in the region $-\eta\Delta/2 < E < \eta\Delta/2+\omega_c$. Then we cut the contour at $E=\pm\infty$ and separate it into two pieces C_1+C_3 and C_2+C_4. Each piece has a part which runs along the real axis, either above or below, and connects to the large semicircle of radius R. When $R\to\infty$, the contour integrals on the two semicircles are zero. So the contour integral in Eq. (A1) becomes

$$\begin{aligned}\sum_E \frac{|x(E)|^2}{E-iP} &= \frac{1}{2\pi i}\oint_{C_1+C_2} \frac{dE}{\left(E-\frac{1}{2}\eta\Delta-\sum_k \frac{V_k^2}{E+\frac{1}{2}\eta\Delta-\omega_k}\right)(E-iP)} \\ &= \frac{1}{2\pi i}\oint_{C_1+C_3} \frac{dE}{\left(E-\frac{1}{2}\eta\Delta-\sum_k \frac{V_k^2}{E+\frac{1}{2}\eta\Delta-\omega_k}\right)(E-iP)} + \frac{1}{2\pi i}\oint_{C_2+C_4} \frac{dE}{\left(E-\frac{1}{2}\eta\Delta-\sum_k \frac{V_k^2}{E+\frac{1}{2}\eta\Delta-\omega_k}\right)(E-iP)}.\end{aligned} \tag{A2}$$

The contours C_1+C_3 and C_2+C_4 contain the pole at $E=iP$ and the residue of it is

$$\sum_E \frac{|x(E)|^2}{E-iP} = -\frac{1}{iP-\frac{1}{2}\eta\Delta-\sum_k \frac{V_k^2}{iP+\frac{1}{2}\eta\Delta-\omega_k}}. \tag{A3}$$

[1] Filippo Troiani, Ulrich Hohenester, and Elisa Molinari, Phys. Rev. B **62**, R2263 (2000).
[2] E. Biolatti, I. D'Amico, P. Zanardi, and F. Rossi, Phys. Rev. B **65**, 075306 (2002).
[3] P. Bertet, I. Chiorescu, G. Burkard, K. Semba, C. J. P. M. Harmans, D. P. DiVincenzo, and J. E. Mooij, Phys. Rev. Lett. **95**, 257002 (2005).
[4] I. Chiorescu, Y. Nakamura, C. J. P. M. Harmans, and J. E. Mooij, Science **299**, 1869 (2003).
[5] J. Claudon, F. Balestro, F. W. J. Hekking, and O. Buisson, Phys. Rev. Lett. **93**, 187003 (2004).
[6] T. Duty, D. Gunnarsson, K. Bladh, and P. Delsing, Phys. Rev. B **69**, 140503(R) (2004).
[7] S. Gardelis, C. G. Smith, J. Cooper, D. A. Ritchie, E. H. Linfield, Y. Jin, and M. Pepper, Phys. Rev. B **67**, 073302 (2003).
[8] L. C. L. Hollenberg, A. S. Dzurak, C. Wellard, A. R. Hamilton, D. J. Reilly, G. J. Milburn, and R. G. Clark, Phys. Rev. B **69**, 113301 (2004).
[9] T. Hayashi, T. Fujisawa, H. D. Cheong, Y. H. Jeong, and Y. Hirayama, Phys. Rev. Lett. **91**, 226804 (2003).
[10] J. Gorman, E. G. Emiroglu, D. G. Hasko, and D. A. Williams, Phys. Rev. Lett. **95**, 090502 (2005).
[11] T. H. Stievater, Xiaoqin Li, D. G. Steel, D. Gammon, D. S. Katzer, D. Park, C. Piermarocchi, and L. J. Sham, Phys. Rev. Lett. **87**, 133603 (2001).
[12] L. Besombes, J. J. Baumberg, and J. Motohisa, Phys. Rev. Lett. **90**, 257402 (2003).
[13] Yu. A. Pashkin, T. Yamamoto, O. Astafiev, Y. Nakamura, D. V. Averin, and J. S. Tsai, Nature (London) **421**, 823 (2003).
[14] A. Zrenner, E. Beham, S. Stufler, F. Findeis, M. Bichler, and G. Abstreiter, Nature (London) **418**, 612 (2002).
[15] B. Krummheuer, V. M. Axt, and T. Kuhn, Phys. Rev. B **65**, 195313 (2002).
[16] Milena Grifoni, Maura Sassetti, J. Stockburger, and Ulrich Weiss, Phys. Rev. E **48**, 3497 (1993).
[17] H. Jirari and W. Pötz, Phys. Rev. A **74**, 022306 (2006).
[18] Milena Grifoni, Maura Sassetti, Peter Hänggi, and Ulrich Weiss, Phys. Rev. E **52**, 3596 (1995).
[19] Ludwig Hartmann, Igor Goychuk, Milena Grifoni, and Peter Hänggi, Phys. Rev. E **61**, R4687 (2000).
[20] Dmitrii E. Makarov and Nancy Makri, Phys. Rev. E **52**, 5863 (1995).
[21] Feng Shuang, Chen Yang, Houyu Zhang, and Y. J. Yan, Phys. Rev. E **61**, 7192 (2000).
[22] P. Silvestrini and L. Stodolsky, Phys. Lett. A **280**, 17 (2001).
[23] T. Brandes and T. Vorrath, Phys. Rev. B **66**, 075341 (2002).
[24] Milena Grifoni and Peter Hänggi, Phys. Rep. **304**, 229 (1998).
[25] H. Zheng, Eur. Phys. J. B **38**, 559 (2004); Zhuo-Jie Wu, Ka-Di Zhu, Xiao-Zhong Yuan, Yi-Wen Jiang, and Hang Zheng, Phys. Rev. B **71**, 205323 (2005); F. Guinea, V. Hakim, and A. Muramatsu, *ibid.* **32**, 4410 (1985).
[26] Marlan O. Scully and M. Suhail Zubairy, *Quantum Optics* (Cambridge University Press, Cambridge, England, 1997).
[27] Gerald D. Mahan, *Many-Partical Physics* (Plenum, New York, 1990).
[28] Milena Grifoni, Manfred Winterstetter, and Ulrich Weiss, Phys. Rev. E **56**, 334 (1997).
[29] D. Vion, A. Aassime, A. Cottet, P. Joyez, H. Pothier, C. Urbina, D. Esteve, and M. H. Devoret, Science **296**, 886 (2002).
[30] K. Shiokawa and B. L. Hu, Phys. Rev. A **70**, 062106 (2004).